IA*VSD*

Taylor & Francis
Taylor & Francis Group

Lap time optimisation of a racing go-kart

Roberto Lot[a] and Nicola Dal Bianco[b]

[a]Engineering and the Environment, University of Southampton, Southampton, UK;
[b]Dipartimento di Inggneria Industriale, Universit degli Studi di Padova, Padova, Italy

ABSTRACT

The minimum lap time optimal control problem has been solved for a go-kart model. The symbolic algebra software Maple has been used to derive equations of motion and an indirect method has been adopted to solve the optimal control problem. Simulation has been successfully performed on a full track lap with a multibody model endowed with seven degrees of freedom. Geometrical and mechanical characteristics of a real kart have been measured by a lab test to feed the mathematical model. Telemetry recorded in an entire lap by a professional driver has been compared to simulation results in order to validate the model. After the reliability of the optimal control model was proved, the simulation has been used to study the peculiar dynamics of go-karts and focus to tyre slippage dynamics, which is highly affected by the lack of differential.

1. Introduction

Optimal control problems applied to racing vehicle are nowadays widely used to simulate and predict the performance on racing tracks. Examples can be found for rally cars,[1] Formula 1 cars [2] and motorcycles.[3,4] However, in the literature there is a lack of optimal control analysis regarding go-karts. Go-karts are four-wheeled vehicle which, unlike cars, do not have suspensions nor differential. Therefore, the dynamics of karts is significantly different from that of other four-wheeled vehicles. The absence of rear axle differential makes the rear wheels to have a strictly correlated longitudinal slip and this characteristic makes it more difficult for a kart to turn than cars. Indeed, when turning at a constant speed, the rear inner tyre has a positive slip, while the rear outer tyre has a negative one; thus, longitudinal forces that tend to oppose to cornering are generated. In order to reduce this effect, the inner rear wheel should be unloaded as much as possible: it is quite usual to see expert drivers lifting up such a wheel while cornering. The frame stiffness and steering geometry are the most important parameters affecting this phenomenon; moreover, the absence of suspensions makes the tyres and frame absorb all shocks induced by road unevenness. Thus, kart frame stiffness becomes a key feature that profoundly affects kart performance, as highlighted in [5] through a multibody simulated analysis and a comparison with experimental data; this study was focused on circular trajectories at a constant speed only.

CONTACT Roberto Lot ✉ roberto.lot@soton.ac.uk

In this work, kart dynamics have been studied with the use of optimal control simulations of an entire circuit lap. The mathematical model of the go-kart has been developed with the use of a symbolic algebra software (MBSymba [6]), and then translated into an optimal control problem with third-part libraries (XOptima and Mechatronix). Such libraries use an indirect formulation to solve the optimal control problem, which has been demonstrated to be effective for such purposes.[7,8]

Simulations have been carried out on the track 'Pista Azzurra', in Jesolo (near Venice), and the results have been validated by comparison with experimental data acquired on the same track. Once the reliability of the model was confirmed, we analysed the dynamics of the kart when treading a turn with particular attention to tyre slippage and how the lack of differential requires high lateral load transfer in order to minimise manoeuvre time.

In the following section, the mathematical model of the kart is described. Then, in Section 3, the optimal control formulation is presented. In Section 4, one model validation is illustrated, including the kart analysis in the laboratory, the data acquiring and the telemetry-simulation comparison. Finally, in Section 5 the analysis of kart dynamics on a turn is presented.

2. Mathematical model of the go-kart

A go-kart is a four-wheeled, rear axle traction vehicle whose distinguishing features are the absence of the suspensions system and differential. Since the vehicle has four contact points with the road, it is hyperstatic. Therefore, the load distribution on each tyre depends on the tyre radial compliance as well as the compliance of the chassis, which is quite deformable. The absence of the differential on the traction axle makes any cornering manoeuvre problematic. Indeed, while cornering, the inner rear wheel has a smaller forward velocity, but the same spin velocity than the outer one. Thus, the inner longitudinal slip is bigger than the outer one, which leads to a yaw torque opposite to the yaw rate. Since the longitudinal force is approximately proportional both to the longitudinal slip and to the tyre load, to reduce such an undesired effect, the vertical load of the inner wheel should be as low as possible and ideally null. This condition may be obtained by designing a proper combination of tyres and chassis stiffness, as well as steering system geometry. Steering geometry indeed plays an important role in load transfers: due to the particular linkages between front wheels and chassis, when steering the inner front tyre gets pulled down by a quantity proportional to the steering angle, while the outer front tyre is lifted up by the same amount. Thus, part of the vertical load is transferred to the front inner wheel and the rear inner one gets more – if not completely – unloaded. Such essential features are fully embraced in the mathematical model of the vehicle, as depicted in Figure 1. The inertia of the vehicle (chassis, engine, tanks, steering, wheels, etc.) is modelled with a single rigid body. Indeed, we are not interested in vehicle vibration nor in any high-frequency dynamics. The mass and inertia of the rider are also incorporated in such a rigid body, since the seat is very stiff and the rider body is constricted. Some racing riders are still able to partially move their torso while cornering, however, this effect is not so relevant and it is completely neglected here. To capture the actual distribution of vertical tyres load, the chassis compliance is modelled by using four vertical translation springs that ideally connect any wheel centre to the chassis, while other four vertical translation springs connect wheel centres to the ground and represent tyres radial stiffness. Two additional springs connecting the right and the left
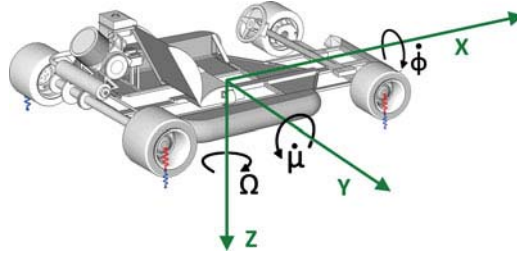
Figure 1. Go-kart model: the six degrees of freedom of the chassis are highlighted. The go-kart coordinate system is represented by the green axes. Black arrows and Greek letters indicate the rotational dof around the main axes. Red springs represent the reduced vertical stiffness of the chassis, while blue ones the tyre radial stiffness. Anti-roll bars (not represented) connect the left and right joint points between chassis and tyre springs.

wheel of each axle take into account for the anti-roll bars. The 125cc go-kart studied in this article was equipped with rear brake only, so the spin dynamics of the rear axle is included into the model, while the front axle is neglected. According to this description, the vehicle model has a total of seven degrees of freedom (dof), six of them associated with the vehicle gross motion and the latter associated with the rear axle spin rotation.

2.1. Newton's equations

The equations of motion have been derived by using `MBSymba`, which is an object-oriented language for the modelling of multibody systems and the automatic generation of the equations of motion.[6] The modelling procedure consists in the description of the multibody system by defining objects such as points, vectors, rigid bodies, forces and torques, and the relationships among them. In particular, it is possible to define which variables are small (infinitesimal) and which are not. Once the system has been modelled, the equations of motion are automatically derived, avoiding any human error. The Newton and Euler equations have been derived with respect to a coordinate system that is fixed to the go-kart body, except for having zero roll and pitch angles.

For a vehicle running on an horizontal, planar road surface, Newton's equations which describe the vehicle translation, respectively, along the longitudinal, lateral and vertical directions are

$$m(\dot{u} - \Omega v) = S_{rl} + S_{rr} - \left(F_{fl} + F_{fr}\right)\sin\delta - \frac{1}{2}\rho C_d A u^2, \tag{1a}$$

$$m\left(\dot{v} + \Omega u\right) = F_{rl} + F_{rr} + \left(F_{fl} + F_{fr}\right)\cos\delta, \tag{1b}$$

$$m\ddot{z} = mg - \left(N_{fl} + N_{fr} + N_{rl} + N_{rr}\right), \tag{1c}$$

where u and v are, respectively, the longitudinal and lateral speed of the vehicle centre of gravity (CoG), while z is the CoG vertical displacement with respect to the static equilibrium position, δ is the front wheel steering angle (assumed to be equal for both wheels), Ω is the yaw velocity, N_{as}, F_{as}, S_{as} are, respectively, the vertical, lateral and longitudinal force of each tyre, where $a \in \{r, f\}$ indicates either the rear axle, r, or the front one, f, and $s \in \{l, r\}$

Table 1. Vehicle parameters.

Symbol	Value	Units	Description
h	0.250	m	[m]Centre of gravity (CoG) height
a	0.645	m	[m]Distance between the front axle and the vehicle CoG
b	0.400	m	[m]Distance between the rear axle and the vehicle CoG
p	1.045		[m]Wheelbase
$2t_f$	1.055	m	[m]Front track
$2t_r$	1.200	m	[m]Rear track
β	0.058	m/rad	[m]Front wheel hub displacement to steering angle ratio
m	165	kg	[m]Vehicle mass (rider included)
I_{xx}	20	kg m^2	[e]Roll moment of inertia
I_{yy}	15	kg m^2	[e]Pitch moment of inertia
I_{zz}	25	kg m^2	[e]Yaw moment of inertia
I_{xz}	5	kg m^2	[e]Mixed moment of inertia
I_r	0.2	kg m^2	[e]Spin inertia of the rear axle
ρ	1.2	kg/m^3	Air density
C_dA	0.7	m^2	[e]Drag surface coefficient
ks_r	60e3	N/m	[m]Rear chassis stiffness (vertical displacements)
ks_f	17.7e3	N/m	[m]Front chassis stiffness (vertical displacements)
kj_r	0	N/m	Rear anti-roll bar stiffness
kj_f	0	N/m	Front anti-roll stiffness
kt_r	61.3e3	N/m	[m]Rear tyres radial stiffness
kt_f	64.5e3	N/m	[m]Front tyres radial stiffness
ct_r	1.0e3	N s/m	[e]Rear tyres radial damping
ct_f	1.0e3	N s/m	[e]Front tyres radial damping
r_r	0.139	m	[m]Rear tyres rolling radius
T_{max}	17.6	N m	[m]Maximum engine torque (@10,250 rpm)
P_{max}	20.1	kW	[m]Maximum engine power (@11,500 rpm)

Notes: [m]: Measured value, [e]: Estimated value, [f]: Fitted value.

indicates either the left side, l, or the right one, r. Finally, model parameters are described in Table 1.

Since tyres and chassis are stiff, it is reasonable to assume that the chassis pitch μ, roll ϕ and vertical displacement z are infinitesimal, as well as their time derivatives. Therefore, the equations of motion with respect to the roll, pitch and yaw rotation axis are

$$m[\dot{v}h + (h - z)\Omega u] + I_{xx}\ddot{\phi} - (I_{yy} - I_{zz} + I_{xx})\Omega\dot{\mu} - (I_{yy} - I_{zz})\Omega^2\phi$$
$$-(I_{xx} - I_{zz})\dot{\Omega}\mu - I_{xz}\dot{\Omega} = t_f(N_{fl} - N_{fr}) + t_r(N_{rl} - N_{rr}), \tag{2a}$$

$$m[(z - h)\dot{u} + h\Omega v] + I_{yy}\ddot{\mu} + (I_{yy} - I_{zz} + I_{xx})\Omega\dot{\phi} - (I_{xx} - I_{zz})\Omega^2\mu$$
$$+(I_{yy} - I_{zz})\dot{\Omega}\phi - I_{xz}\Omega^2 = a(N_{fr} + N_{fl}) - b(N_{rr} + N_{rl}) - \frac{1}{2}\rho C_dAu^2(z - h), \tag{2b}$$

$$I_{zz}\dot{\Omega} - I_{xz}(\ddot{\phi} + 2\mu\dot{\Omega} + 2\dot{\mu}\Omega) = a(F_{fl} + F_{fr})\cos\delta - b(F_{rr} + F_{rr})$$
$$+t_f(F_{fr} - F_{fl})\sin\delta + t_r(S_{rl} - S_{rr}). \tag{2c}$$

It is worth pointing out that angular momenta have been evaluated with respect to the vertical projection of the CoG onto the road plane. This choice simplifies the roll (2a) and pitch (2b) equations by avoiding the presence of any term related to longitudinal or lateral tyre forces.

Finally, the model is completed by the following rear axle spin equation of motion:

$$I_r\dot{\omega}_r = T_r - S_{rr}(r_r - w_{rr}) - S_{rl}(r_r - w_{rl}), \tag{3}$$

185 where ω_r is the axle spin velocity, r_r is the rear tyre radius, w_{rr} and w_{rr} are rear right and
186 rear left tyre deformations, respectively, and T_r is the axle torque due to either the engine
187 ($T_r > 0$) or the brake ($T_r < 0$). The inertia I_r includes all parts connected to the shaft
188 (wheels, disk brake, etc.) as well as the equivalent inertia of the engine, which is connected
189 to the rear axle by a fixed ratio chain transmission.
190
191
2.2. Tyres model
192
193 Since the vehicle has four contact points with the road, it is not possible to determine the
194 tyre vertical load unless the compliances of tyres and chassis are considered. In a kart, tyre
195 stiffness is generally 3–5 times greater than chassis stiffness; however, in this model only
196 their combined stiffness is considered. Indeed, free vibration frequencies of the chassis with
197 attached wheels are far faster than the eigenfrequencies of vehicle gross motion, so chassis
198 and wheels may be considered as a unique rigid body which is attached to the road by
199 means of massless springs and dampers. According to these assumptions, for each wheel
200 the load force due to tyre deformation has been made equal to the vertical force due to
201 chassis deformation, as shown in the following formulas. Tyre deformations are given by
202
203
204 $$w_{fr} = z + s_{fr} - a\mu + t_f\phi + \beta\,\delta,$$
205 $$w_{fl} = z + s_{fl} - a\mu - t_f\phi - \beta\,\delta,$$
206 $$w_{rr} = z + s_{rr} + b\mu + t_r\phi,$$
207 $$w_{rl} = z + s_{rl} + b\mu - t_r\phi,$$
208
$$(4)$$
209 where s are frame vertical deformations and $\pm\beta\delta$ is the linear approximation of the kine-
210 matic relationship that links the vertical motion of the wheel centre to the steering angle (in
211 other words β is the ratio between wheel vertical displacement and steering angle). Then,
212 by making tyre loads equal to chassis deformation forces on each wheel:
213
214 $$s_{rr}k_{sr} + (s_{rr} - s_{rl})k_{jr} + w_{rr}k_{tr} = 0,$$
215 $$s_{rl}k_{sr} + (s_{rl} - s_{rr})k_{jr} + w_{rl}k_{tr} = 0,$$
216 $$s_{fr}k_{sf} + (s_{fr} - s_{fl})k_{jf} + w_{fr}k_{tf} = 0,$$
217 $$s_{fl}k_{sf} + (s_{fl} - s_{fr})k_{jf} + w_{fl}k_{tf} = 0,$$
218
$$(5)$$
219
220 where k_{sf}, k_{sr} are the chassis stiffness at the front and rear axles, and k_{jr} and k_{jf} are the rear
221 and front anti-roll bar stiffness. In Equations (5), the first terms represent the force due
222 to chassis deformations, the second terms are the force of the anti-roll bars and the last
223 terms stand for tyres deformation loads. Once the expressions for s are obtained, they can
224 be substituted into the tyre deformation expressions that become
225
226
227 $$w_{rr} = \frac{k_{sr}(\mu b + \phi t_r + z)}{k_{sr} + k_{tr}} + \frac{2\phi k_{tr}t_r k_{jr}}{(k_{sr} + k_{tr})(2k_{jr} + k_{sr} + k_{tr})},$$
228
229 $$w_{rl} = \frac{k_{sr}(\mu b - \phi t_r + z)}{k_{sr} + k_{tr}} - \frac{2\phi k_{tr}t_r k_{jr}}{(k_{sr} + k_{tr})(2k_{jr} + k_{sr} + k_{tr})},$$
230

$$w_{fr} = -\frac{k_{sf}(\mu a - \beta\delta - \phi t_f - z)}{k_{sf} + k_{tf}} + \frac{2k_{jf}k_{tf}(\beta\delta + \phi t_f)}{(k_{sf} + k_{tf})(2k_{jf} + k_{sf} + k_{tf})}, \tag{6}$$

$$w_{fl} = -\frac{k_{sf}(\beta\delta + \mu a + \phi t_f - z)}{k_{sf} + k_{tf}} - \frac{2k_{jf}k_{tf}(\beta\delta + \phi t_f)}{(k_{sf} + k_{tf})(2k_{jf} + k_{sf} + k_{tf})}.$$

From these expressions, it can be noticed that tyre deformations are given by two terms: the first is that of a totally rigid chassis with tyre radial stiffness given by the series of chassis and tyre springs, and the second term is due to the anti-roll bar and proportional to the stiffness of the bars. Such expressions for tyre deformations have been substituted into tyre loads in order to algebraically remove the degrees of freedom of chassis deformations. As shown in Equation (7), a damping term proportional to the tyre deformation rate has been added in the calculus of tyre loads. Such a term, even if it is negligible for the dynamics of the vehicle, has been inserted to eliminate undesired oscillations in the simulation results. Finally, since while cornering the rear inner wheel may lift up and loose the contact with the ground, the rear tyre load expressions have been saturated accordingly. Thus:

$$N_{rr} = \max(0, k_{tr}w_{rr} + c_{tr}\dot{w}_{rr}),$$
$$N_{rl} = \max(0, k_{tr}w_{rl} + c_{tr}\dot{w}_{rl}),$$
$$N_{fr} = k_{tf}w_{fr} + c_{tf}\dot{w}_{fr}, \tag{7}$$
$$N_{fl} = k_{tf}w_{fl} + c_{tf}\dot{w}_{fl},$$

where ct_r, ct_f are rear and front tyre radial damping and $\max(x, y)$ is a function that returns the maximum between x and y. For the sake of legibility, the tyre deformation expressions (Equation (6)) have not been substituted into previous equations. Lateral tyres forces and longitudinal tyres forces are calculated according to the Magic formula [9] as a function of tyre vertical load N, sideslip angle λ and longitudinal slip κ. In particular, sideslips may be calculated as follows:

$$\lambda_{rr} = -\arctan\left(\frac{v - \Omega b}{u - \Omega t_r}\right),$$
$$\lambda_{rl} = -\arctan\left(\frac{v - \Omega b}{u + \Omega t_r}\right),$$
$$\lambda_{fr} = \delta - \arctan\left(\frac{v + \Omega a}{u - \Omega t_f}\right), \tag{8}$$
$$\lambda_{fl} = \delta - \arctan\left(\frac{v + \Omega a}{u + \Omega t_f}\right).$$

Longitudinal slips are calculated for the rear axle only:

$$\kappa_{rr} = \frac{\omega_r r_r}{u - \Omega t_r} - 1,$$
$$\kappa_{rl} = \frac{\omega_r r_r}{u + \Omega t_r} - 1. \tag{9}$$

Since the time lag which is present in the generation of lateral forces due to lateral compliance of tyre carcass is known to have a remarkable influence on the vehicle stability, such

a phenomenon is modelled as a first-order relaxation equation [9] for each tyre:

$$\frac{\sigma_r}{u - \Omega t_r}\dot{F}_{rr} + F_{rr} = F_{\mathrm{magic},r}(N_{rr}, \lambda_{rr}, \kappa_{rr}),$$

$$\frac{\sigma_r}{u + \Omega t_r}\dot{F}_{rl} + F_{rl} = F_{\mathrm{magic},r}(N_{rl}, \lambda_{rl}, \kappa_{rl}),$$

$$\frac{\sigma_f}{(u - \Omega t_f)\cos\delta + (v + \Omega a)\sin\delta}\dot{F}_{fr} + F_{fr} = F_{\mathrm{magic},f}(N_{fr}, \lambda_{fr}, \kappa_{fr}),$$

$$\frac{\sigma_f}{(u + \Omega t_f)\cos\delta + (v + \Omega a)\sin\delta}\dot{F}_{fl} + F_{fl} = F_{\mathrm{magic},f}(N_{fr}, \lambda_{fl}, \kappa_{fl}).$$

(10)

On the real axle, small spin inertia leads to fast dynamics and hence longitudinal forces are calculated without any time lag:

$$S_{rr} = S_{\mathrm{magic}}(N_{rr}, \lambda_{rr}, \kappa_{rr}),$$

$$S_{rl} = S_{\mathrm{magic}}(N_{rr}, \lambda_{rl}, \kappa_{rl}),$$

(11)

where $S_{\mathrm{magic},r}$, $F_{\mathrm{magic},r}$ and $F_{\mathrm{magic},f}$ are the functions returning, respectively, the rear longitudinal, rear lateral and front lateral tyre forces (front and rear tyres have different parameters). The Pacejka Magic Formula Tyre Model ([9], chapter 4) has been used in $S_{\mathrm{magic},r}$, $F_{\mathrm{magic},r}$ and $F_{\mathrm{magic},f}$, but the dependence on the tyre roll angle has been neglected. All the coefficients used in these formulas are listed in the appendix; the parameters that do not appear in the table in the appendix have been set to zero (or to one, in the case of scaling coefficients). This is because, as described in Section 4.1, only the tyres lateral stiffness have been measured in lab tests; thus, we used only the smallest number of parameters in Pacejka's magic formulas.

2.3. Road and vehicle tracking

Real roads are similar to strips: they are long and narrow. According to this idea, Figure 2 illustrates a string-shaped road, which may be described by specifying the (x, y) coordinates of the middle line $\mathcal{C}$ and the lateral width. As explained in [10], the most effective way to describe the road centre is the curvilinear abscissa approach, which makes it possible to define $\mathcal{C}$ by only giving the expression of the line curvature κ as a function of the line length s. Then, the road heading angle Θ as well as x, y coordinates may be calculated by integrating the curvature as follows:

$$\frac{\mathrm{d}}{\mathrm{d}s}\Theta = \kappa(s),$$

$$\frac{\mathrm{d}}{\mathrm{d}s}x = \cos\Theta,$$

$$\frac{\mathrm{d}}{\mathrm{d}s}y = \sin\Theta.$$

(12)

The advantage of this approach becomes evident while reminding that real roads and tracks are commonly designed in terms of straight segments (null curvature) which are connected
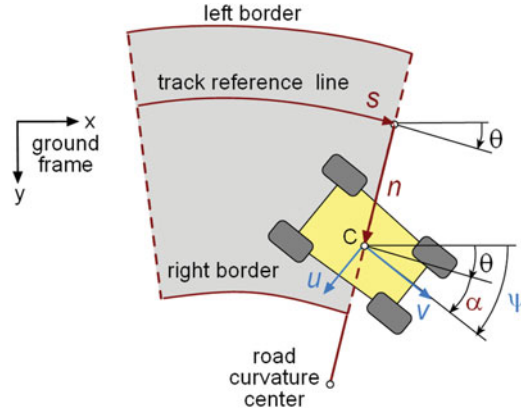
Figure 2. Road tracking.

to circular arcs (constant curvature) by means of clothoids (which curvature varies linearly). Indeed, while driving the steering angle is approximately proportional to the road and hence it is essential to avoid any discontinuity in the curvature.

The advantage of the curvilinear coordinates approach becomes even more significant when it is applied to track the position and orientation of the vehicle as shown in Figure 2, where s and n are, respectively, the longitudinal and lateral position on the road strip, while α is the vehicle heading relative to the road (in other words, α is the angle between the road mid-line direction and the x-axis fixed on the vehicle). The calculus of the vehicle forward and lateral speed, as well as yaw velocity, yields

$$\dot{s} = \frac{u \cos \alpha - v \sin \alpha}{1 - n \kappa(s)}, \tag{13a}$$

$$\dot{n} = u \sin \alpha + v \cos \alpha, \tag{13b}$$

$$\dot{\alpha} = \Omega - \frac{u \cos \alpha - v \sin \alpha}{1 - n \kappa(s)} \kappa(s). \tag{13c}$$

Equations (13) track vehicle position and orientation relative to the road by simply integrating vehicle speeds together with road curvature, so vehicle lateral position n and relative heading α are immediately available as state variables. This is a remarkable advantage in comparison to the Cartesian coordinate approach, which requires separate algorithms to estimate such information.

2.4. First-order formulation

Newton's equations (1) and (2) may be immediately reduced to the first order by introducing auxiliary variables for the relevant chassis speeds:

$$\dot{z} = z_{\text{dot}},$$
$$\dot{\phi} = \omega_{\phi}, \tag{14}$$
$$\dot{\mu} = \omega_{\mu}.$$

At this point, Equations (1)–(3), (10), (13) and (14) and their subordinate expressions completely describe the go-kart dynamics as a system of 17 first-order differential equations with as many state variables and 2 inputs, respectively, the rear axle torque T_r, which (mainly) control the longitudinal dynamics, and the steering angle δ, which (mainly) control the lateral dynamics. However, to avoid unrealistic jerky manoeuvres, it is necessary to consider that human drivers have a limited rate of change of control variables and experimental results show that humans optimise their driving actions minimising the longitudinal and lateral jerks.[11] For this reason, it is assumed that the steering angle is not controlled directly, but via its time derivative, as follows:

$$\dot{\delta} = \omega_\delta,$$
$$\dot{T}_r = mr_r j_u,$$

(15)

where ω_δ is the steering speed, which is approximately related to the lateral jerk and j_u (approximately) corresponds to the longitudinal jerk.

In conclusion, the vehicle dynamics is described by means of a set of two inputs:

$$\boldsymbol{u} = \{\omega_\delta, j_u\}^{\mathrm{T}},$$

(16)

plus 19 state variables:

$$\boldsymbol{x} = \{s, n, \alpha, z, \phi, \mu, u, v, z_{\mathrm{dot}}, \Omega, \omega_\phi, \omega_\mu, \omega_r, F_{rr}, F_{rl}, F_{fr}, F_{fl}, \delta, T_r\}^{\mathrm{T}}$$

(17)

and as many implicit first-order differential equations, which may be abbreviated to:

$$\hat{A}(\boldsymbol{x})\dot{\boldsymbol{x}} = \hat{f}(\boldsymbol{x}, \boldsymbol{u}),$$

(18)

where matrix $\tilde{A}$ is invertible provided that $u > 0$, i.e. the vehicle never stops, and $n < 1/\kappa(s)$, i.e. the vehicle never passes over the local curvature centre of the road.

3. Optimal control problem

3.1. Vehicle dynamics in curvilinear abscissa domain

The minimum lap time problem consists, as previously said, in finding the vehicle control inputs that minimise the time T necessary to move the vehicle along the track from the starting line to the finish one. Therefore, the curvilinear abscissa s varies between fixed initial point $s = 0$ and end point $s = L$, while the final value T of the independent variable t is unknown. For this reason, it is convenient to change the independent variable from t to s in the equations of motion (18). Such a variable change is based on the following derivation rule:

$$\dot{\boldsymbol{x}} = \frac{\mathrm{d}\boldsymbol{x}}{\mathrm{d}t} = \frac{\mathrm{d}\boldsymbol{x}}{\mathrm{d}s}\frac{\mathrm{d}s}{\mathrm{d}t} = \boldsymbol{x}'\dot{s} = \boldsymbol{x}'v.$$

(19)

The time domain equations (18) are then transformed into the space domain as follows:

$$v\tilde{A}\boldsymbol{x}' = \tilde{f}(\boldsymbol{x}, \boldsymbol{u}).$$

(20)

However, the variable change (19) transforms the differential equation (13a) into an algebraic one, that should be eliminated from state equations (20) together with the variable s

which can no more belongs to the state vector $\boldsymbol{x}$. At this point, the variable t is no longer present in the model; however, it can be easily re-introduced by writing Equation (13a) as follows:

$$\frac{\mathrm{d}t}{\mathrm{d}s} = t' = \frac{1}{v} = \frac{1 - n\kappa(s)}{u\cos\alpha - v\sin\alpha}. \tag{21}$$

Summarising, the s-domain state space model has $n = 19$ state variables:

$$\boldsymbol{y} = \{t, n, \alpha, z, \phi, \mu, u, v, w, \Omega, \omega_\phi, \omega_\mu, \omega_r, F_{rr}, F_{rl}, F_{fr}, F_{fl}, \delta, T_r\}^\mathrm{T} \tag{22}$$

and $p = 2$ inputs already defined in Equation (16) but now depend on s, while model equations may be summarised as a set of implicit differential equations:

$$v A \boldsymbol{y}' = \boldsymbol{f}(\boldsymbol{y}, \boldsymbol{u}, s). \tag{23}$$

Equations (23) are not singular only and if only $v > 0$, i.e. the s-domain formulation requires that the vehicle never stops (a condition already required in the t-domain formulation) nor can it revert its direction of travel on the track.

3.2. The minimum lap time problem

The Optimal control problem (OCP) consists in finding the vehicle control inputs that move the vehicle from the starting line $s = 0$ and $t(0) = 0$ to the finish one $s = L$ in the minimum time $T = t(L)$, while satisfying the mechanical equations of motion as well as other inequality constraints (tyres adherence, max power, track width, etc.) and may be formulated as follows:

$$\text{find}: \quad \min_{\boldsymbol{u}\in U} t(L) \tag{24a}$$

$$\text{subject to}: \quad v A \boldsymbol{y}' = \boldsymbol{f}(\boldsymbol{y}, \boldsymbol{u}, s), \quad \boldsymbol{y} \in \mathbb{R}^n, \ \boldsymbol{u} \in \mathbb{R}^p \tag{24b}$$

$$\boldsymbol{\psi}(\boldsymbol{y}, \boldsymbol{u}, s) \leq \boldsymbol{0}, \quad \boldsymbol{\psi} \in \mathbb{R}^m \tag{24c}$$

$$\boldsymbol{b}(\boldsymbol{y}(0), \boldsymbol{y}(L)) = \boldsymbol{0}, \quad \boldsymbol{b} \in \mathbb{R}^{r\leq 2n}, \tag{24d}$$

where Equation (24b) is the state space model already discussed, Equation (24c) are algebraic inequalities that may bound both the state variables and control inputs and Equation (24d) is the set of boundary conditions used to (partially) specify the vehicle state at the beginning and at the end of the manoeuvre.

Inequalities (24c) are used to keep the vehicle inside the admissible range of operating conditions. First of all, all wheels must remain inside the track (see Figure 2). Such a condition for the front right, front left, rear right and rear left wheel can be expressed as

$$n + a\sin(\alpha) + t_f\cos(\alpha) \leq w_r,$$

$$n + a\sin(\alpha) - t_f\cos(\alpha) \geq -w_l,$$

$$n - b\sin(\alpha) + t_r\cos(\alpha) \leq w_r, \tag{25}$$

$$n - b\sin(\alpha) - t_r\cos(\alpha) \geq -w_l,$$

where w_l and w_r are the distance of the left and right border from the track reference line (that might vary along the track), respectively. The propulsive torque on the rear axle T_r is

limited by the maximum engine torque, which is a function of the engine speed $\omega_e = \tau_e \omega_r$, as follows:

$$T_r \leq \tau_e T_e(\tau_e \omega_r). \tag{26}$$

It is not necessary to explicitly restrict tyre longitudinal and lateral forces within their adherence limits; indeed, such constraints are implicitly contained in the saturated Magic formula used in Equations (11) and (10). On the contrary, it is necessary to explicitly prevent vehicle roll-over by imposing the following constraints on the front vertical loads:

$$N_{fr} \geq 0,$$
$$N_{fl} \geq 0. \tag{27}$$

Finally, the control inputs are limited in magnitude as follows:

$$-\omega_L \leq \omega_\delta \leq \omega_L, \tag{28a}$$

$$-j_L \leq j_u \leq j_L. \tag{28b}$$

Equations (25)–(28) form a set of $m = 11$ unilateral constraints of type (24c). The presence of such inequality constraints makes the OCP problem (24) particularly hard to solve. However, it is possible to convert such inequality constraints into penalty terms [7] to be included in the optimality criterion (24a). Each penalty term should be very small (ideally null) when a constraint is satisfied and suddenly should become large as the constraint limit is approached and possibly reached. In conclusion, the OCP problem (24) is replaced with the (almost) equivalent one which does not contain inequality constraints:

$$\text{find}: \quad \min_{\mathbf{u} \in U} t(L) + \sum_{j=1}^{m} \int_0^L W_j(\psi_j(\mathbf{y}, \mathbf{u}, s)) \, \mathrm{d}s \tag{29a}$$

$$\text{subject to}: \quad v A \mathbf{y}' = \mathbf{f}(\mathbf{y}, \mathbf{u}, s) \tag{29b}$$

$$\mathbf{b}(\mathbf{y}(0), \mathbf{y}(L)) = \mathbf{0}. \tag{29c}$$

To complete the problem definition, it is necessary to specify boundary conditions (24d). As the optimisation is made on a closed loop track, it is natural to impose cyclic boundary conditions for all state variables $\mathbf{y}(s)$, except for $t(L)$ which is of course free and under optimisation. The OCP formulation (29) is general and the problem may be solved by using different approaches [12] such as non-linear programming, dynamic programming, and Pontryagin's indirect method, which is the one that has been used in the present paper. Such a method,[13] using Lagrange's multipliers technique, eliminates differential constraints (29b) and transforms the OCP formulation (29) into a functional unconstrained minimisation problem. Then, according to the variational first principle, the stationarity condition of the functional to be minimised leads to a two-point boundary value problem (BVP). Despite the elegance of this well-known technique, it is not straightforward to apply this to complex models as the one presented here. However, the utilisation of computer algebra tools (we used Maple) makes it possible to symbolically derive BVP equations and automatically convert them into a C++ code ready to be compiled, avoiding human errors. Finally, the BVP problem is discretised and numerically integrated using XOPtima, a specialised solver.[8]

4. Experimental test and model validation

In order to provide a validation of the mathematical model by comparison between simulation results with experimental telemetry, a precise measurement of the go-kart characteristic is first necessary. Indeed, the reliability of the simulation is highly affected by the agreement of the data used with real kart properties.

In the following section, the description of the procedure used to measure go-kart characteristics is reported, while in Section 4.2 simulation results are compared to track data.

4.1. Lab tests

The geometry, inertia and compliance of the go-kart, as well as tyre properties, have been measured to feed the simulation model. The geometry of the chassis has been carefully measured by using a 3D coordinate-measuring machine. Weighing balances have been used to measure the go-kart mass and its longitudinal position, the CoG vertical position was estimated by tilting the vehicle until it reached its (unstable) equilibrium position on the two lateral wheels. Such geometric and inertial data was used to build a virtual prototype of the go-kart, which has been used to estimate the moment of inertia as well as to estimate the frame stiffness by means of a FEM analysis. The frame is complex and its representation in terms of few lumped springs used in the vehicle dynamic illustrated Section 2 disregards many degrees of freedom and the correlation of such lumped stiffness to FEM analysis is not trivial. In this case, the focus is on the correct estimation of tyres vertical loads, so the hub points stiffness have been estimated by simultaneously locking three wheels hub and by applying a vertical force on the last one. Vehicle parameters are collected in Table 1. Tyres properties have been measured on the rotating tyre test rig which is available at the department.[14] The identification of the vertical structural stiffness k_{tr}, k_{tf} has been carried out by applying different vertical loads in the range of 0–1500 N both front and rear tyres showed a good linear behaviour. Tyre adherence was measured with a vertical load of 560 N, which is approximately the load of a rear tyre in static conditions. Figure 3 shows the ratio between the lateral force and the vertical load as a function of the sideslip angle, for both the front and the rear tyre. The tyre behaviour in the range of 0–6° of sideslip has been accurately identified, but unfortunately the adherence peak was not reached during measurements; indeed, the friction between the tyre and the test rig were exaggeratedly high (as the tyre test rig was not specifically designed to measure kart tyres). It is worth pointing out that in actual driving conditions the adherence limit remarkably depends on many parameters and in particular on the asphalt characteristics. Hence, the correlation with lab measurement would not be very easy in any case. On the contrary, the cornering stiffness, i.e. the tyre behaviour at low sideslip angles, mainly depends on the tyre carcass characteristics and it is not so much influenced by the tyre–road friction properties.[9,15] For this reason, tyres adherence peak have been adjusted to fit the experimental maximum accelerations (that can be read in Figure 6). Tyre forces that were used for the simulation are reported in Figure 4. Rear tyre normalised lateral force is shown for different values of longitudinal slip to highlight the coupling between lateral and longitudinal forces. For the front tyre, the force is shown only for $\kappa = 0$ because the front tyre's longitudinal slip is not modelled. Tyres adherence values, together with all coefficients of
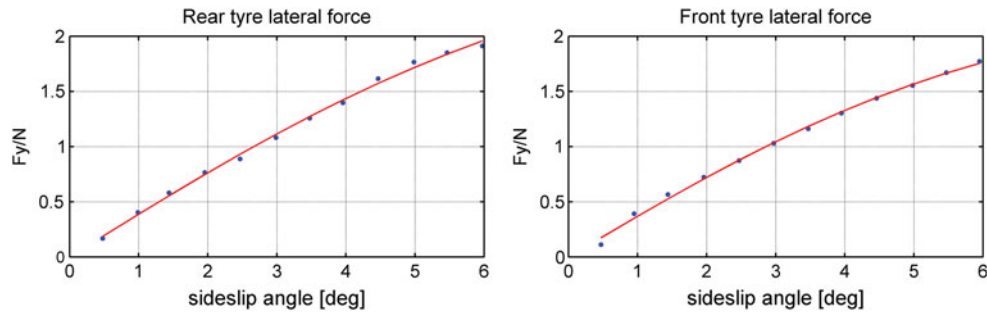
Figure 3. Lateral force of front and rear tyres measured on the test rig. Continuous red lines represent data fit.
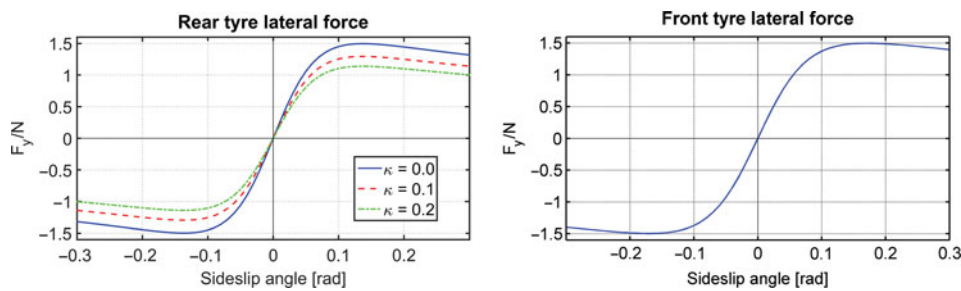

Figure 4. Tyre forces: normalised lateral forces are shown for rear and front tyres at a vertical load of 560 N. For rear tyre the force is shown at different values of longitudinal slip.

Pacejka's magic formula, are summarised in Table A1. The lateral friction peak coefficient (1.50) is significantly higher than longitudinal one (0.90) because in kart tracks thin layers of rubber get often deposited on the asphalt in curves due to high tyre slippage. Thus, turns are characterised by a higher friction coefficient than straights, and this effect can be modelled by considering tyres with greater lateral adherence. Such adherence conditions are confirmed in Section 4.3 by the validation of the model with experimental data. The engine torque curve used in this simulation is the one provide by Iame (www.iame.it).

4.2. Track tests

The go-kart has been equipped with an inertial measurement platform (IMU) composed of three accelerometers and three gyrometers. Moreover, a Hall sensor has been installed on the rear axle to measure the spin velocity and a rotational potentiometer has been installed on the steering system to measure the steering angle. All sensors have been connected to the data logger by means of a dedicated CAN bus. Tests have been carried out at Pista Azzurra (Jesolo), which is a national category race-track 1051 m long with an average width of 8 m. Tests were carried out on a cold day in November, with adherence conditions far from being optimal, by an expert driver who participates in go-kart races at the Italian level. Figures 6(b) and 6(c) highlighted the bounds of both the lateral accelerations $|a_y| < 15\,\text{m/s}^2$ and longitudinal one $-7\,\text{m/s}^2 < a_x < 5\,\text{m/s}^2$. While the traction acceleration is limited by the engine power, lateral and braking accelerations are limited by tyre adherence,

Figure 5. Satellite view of Pista Azzurra with simulation trajectory overlying (yellow line). Numbers inside boxes show the value of the curvilinear abscissa *s* along the track every 100 m. The turn inside the black rectangle is the one analysed in the next chapter.

where lateral adherence is much bigger than the longitudinal one, thanks to the rubber deposits that tyres leave in curve. It is worth pointing out that, most likely, the driver was not able to drive very close to the tyre adherence limit and hence the acceleration bounds are a measure of driver's capability rather than tyre adherence. However, this is not a big issue for the validation of the simulation software, as the focus will be posed on the comparison between speed profile of real and virtual driver, constrained within the same acceleration bounds.

4.3. Validation

The simulation took approximately 230 s on a common laptop equipped with an Intel Core-i7 640M processor. Figure 5 shows a satellite view of the track with the overlying trajectory resulting from the optimal manoeuvring method. The trajectory confirms that the kart remains always within borders of the real track, suggesting that the road has been accurately reproduced. Simulated and experimental time lap are, respectively, 53.575 and 53.580 s. However, this is not an indication of the quality of the simulation since the information on the time lap has been used to fine tune tyre adherence, which has been estimated from measured lateral and longitudinal accelerations. The accuracy of the simulation should be instead evaluated by comparing measured data with simulated ones as they both vary along the track, as reported in Figure 6: dash-dot red lines refer to telemetry data, continuous blue ones to simulation. The simulated speed profile reproduces faithfully the experimental one; there are some slightly discrepancies in the speed at the middle of some turns, where the simulation is sometime faster, other slower. In addition to the simulation errors that are certainly present because of model approximation and parameter inaccuracy, it should be kept into consideration that asphalt was not perfectly dry so some parts of the circuit had a different adherence compared to others. Moreover, the driver
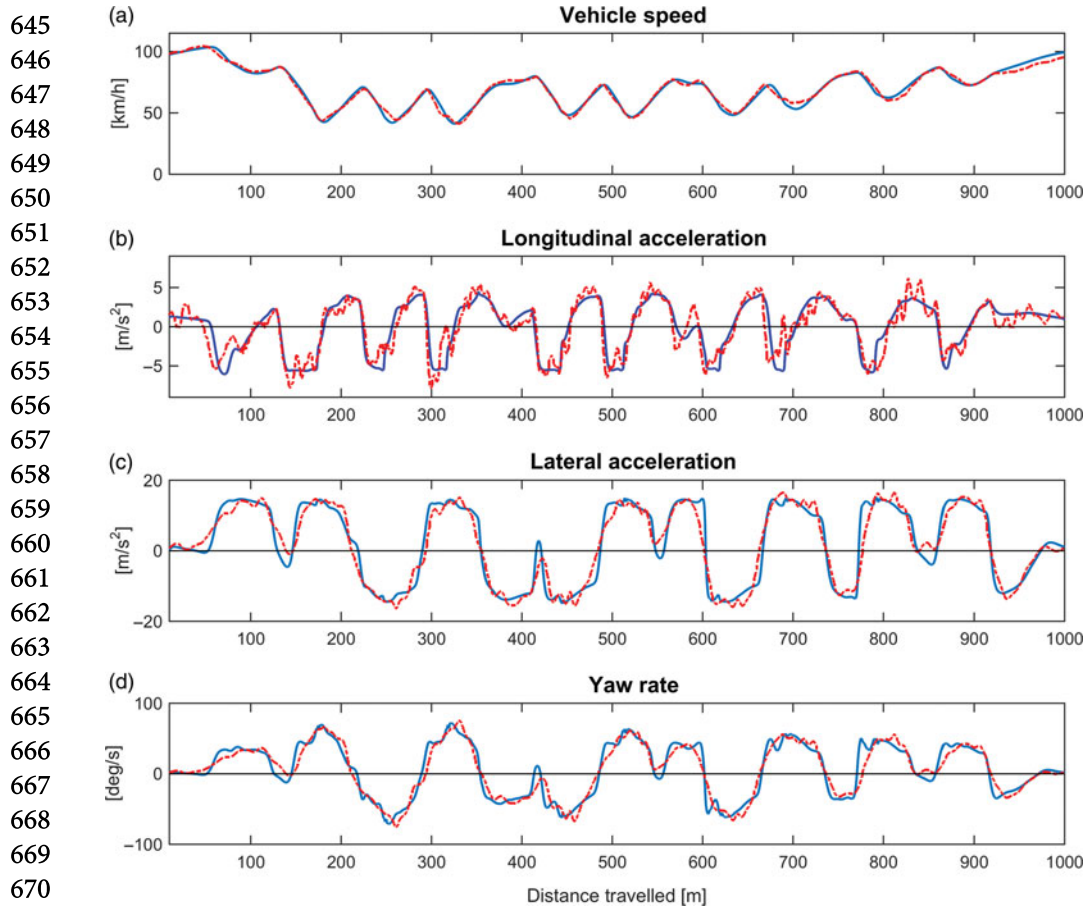
Figure 6. Vehicle gross motion for the full lap: dash-dot red lines refer to telemetry data, continuous blue ones to simulation results.

was very skilled but not professional. So, we think that the accordance between simulation and experiments is excellent. Longitudinal and lateral accelerations also reproduce faithfully the measured trend. Simulated signals are obviously smoother than the experimental ones, due to the absence of every source of unwanted vibrations. For this reason, the peak value of experimental accelerations are higher than the simulated one. The experimental lateral acceleration and yaw rate signal are less affected by external noise with respect to longitudinal acceleration and they have a better correspondence with the corresponding simulated quantities.

Figure 7 shows additional variables that are available for the simulation only and which are quite useful to analyse the go-kart behaviour. Rear tyre longitudinal and lateral slips are reported, respectively, on the first and the second line. As shown in the figure, sideslip angles of rear tyres are quite identical for left and right sides, while for the longitudinal slips there are significant differences. Due to the absence of a differential, such slippage differences are consequences of the yaw motion only. Thus, at a given time only one tyre can have the combination of κ and λ that produces the maximum force: this means that it is
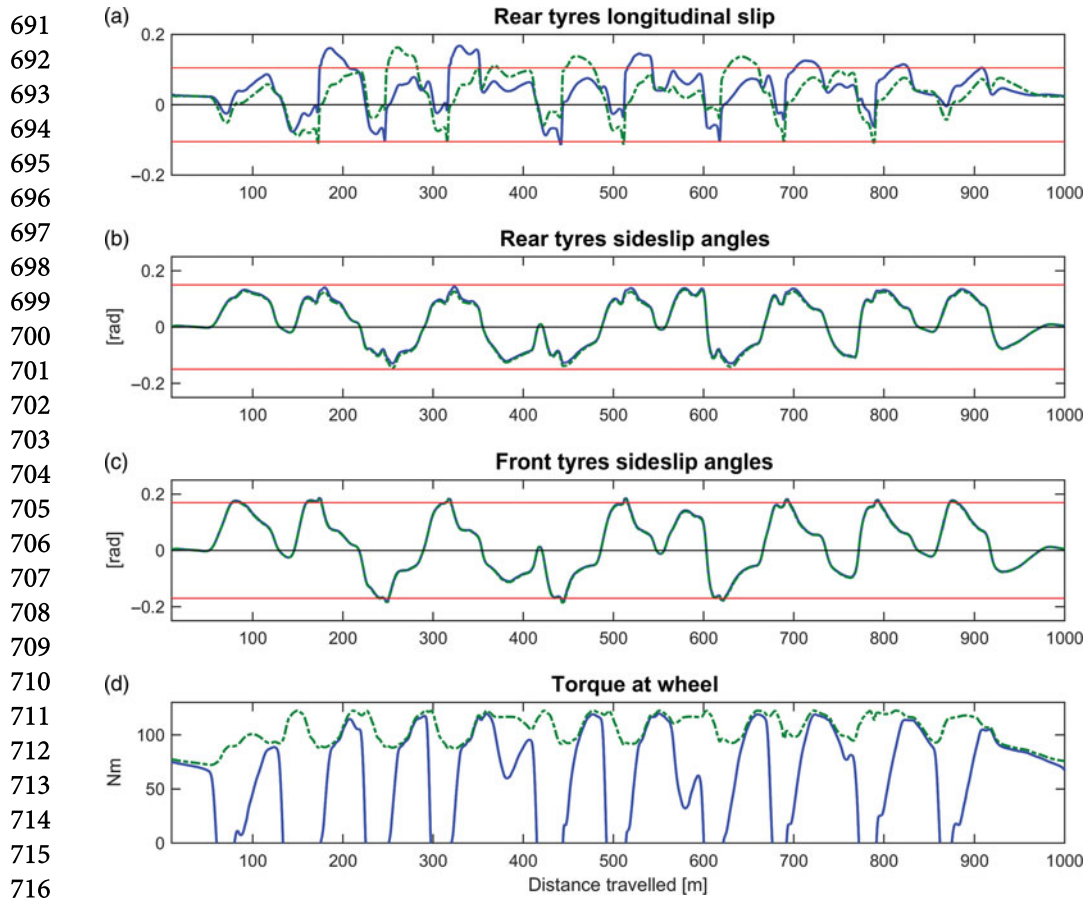
Figure 7. Simulation details: in tyre slip charts, continuous blue lines refer to right tyre, dash-dot green lines to left one. Horizontal red lines represent the value at which the maximum of tyre adherence is reached for a non-combined tyre force. In the chart *d*, the continuous blue line represents the used torque, the dash-dot green one the maximum available torque.

not possible to bring both tyres at adherence limits in the same manoeuvre, and the optimal control obviously tends to engage to the limit (at a longitudinal slip κ of ≈ 0.105) the tyre that has more load, i.e. the one. When it reaches such conditions, the inner one consequently is forced to have a greater slippage and reaches the high slip values (≈ 0.17) that are beyond the maximum of Pacejka's magic formula. Regarding sideslip angles, tyres are never pushed beyond the maximum of the magic formula thanks to the optimality condition. Moreover, only the front tyres go slightly beyond the maximum of lateral adherence (at $\lambda \approx 0.17\,\mathrm{rad}$). This is not in contradiction with the optimality condition because lateral force does not decrease suddenly after the peak (see Figure 4); moreover, keeping the front tyres at a higher steering angle helps the vehicle to brake. The rear tyres instead are limited to lower sideslip angles because their lateral slippage is due only to kart drift angle. However, thanks to the higher sideslip stiffness, the rear tyres get extremely close to their maximum lateral adherence (at $\lambda \approx 0.15\,\mathrm{rad}$). Finally, the last graph reported in Figure 7

737 shows that engine torque represents the limiting factor when traction is required and never
738 exceeds the maximum available power.
739
740
5. Turn analysis
741
742 In order to better understand kart dynamics, this section focuses on in-depth analysis of
743 the vehicle behaviour while running along a particular curve of the entire track, the clock-
744 wise one comprised between 120 and 215 m of the curvilinear abscissa s. This is the turn
745 within black box in Figure 5; the details of the track and the optimal trajectory are shown
746 in Figure 8: the kart reaches the external track borders at the entrance of the curve, then it
747 passes at the apex in the middle of the turn, finally, after exiting the curve, it remains in a
748 central position before approaching the next, counterclockwise turn.
749 The speed profile in Figure 9 shows that the kart starts from a speed of $\approx 85\,\text{km/h}$
750 and brakes to $\approx 45\,\text{km/h}$ with a maximum longitudinal deceleration $a_x \approx -5.5\,\text{m/s}^2$:
751 even if the estimated longitudinal tyre friction is equal to 0.91, the maximum decelera-
752 tion is significantly lower than 0.91 g because the kart has brakes on the rear axle only.
753 Braking deceleration remains nearly constant to its maximum until $s \approx 165\,\text{m}$, then for
754 $165 < s < 185$, a_x grows up to its maximum value of $4\,\text{m/s}^2$. Such acceleration is kept
755 nearly constant while exiting the turn. Lateral acceleration also is kept almost constant
756 at $\approx 13\,\text{m/s}^2$ while turning ($150 < s < 200$). Steering angle, drift angle and yaw rate
757 trends highlight that a small *pendulum* manoeuvre is exploited before the beginning of
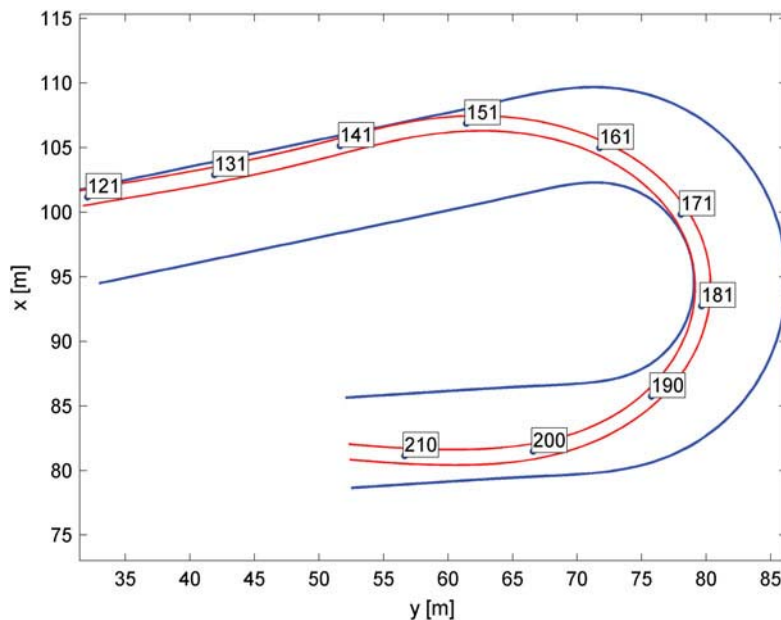758 the turn. Summarising, the manoeuvre can be dividend into three phases that can be
759
760
761
762
763
764
765
766
767
768
769
770
771
772
773
774
775
776
777
778
779

780 **Figure 8.** Turn analysis: optimal trajectory. Red lines represent kart edge trajectories, numbers in rect-
781 angular box show the value of the curvilinear abscissa s. The location of the turn in the circuit is shown
782 in Figure 5.
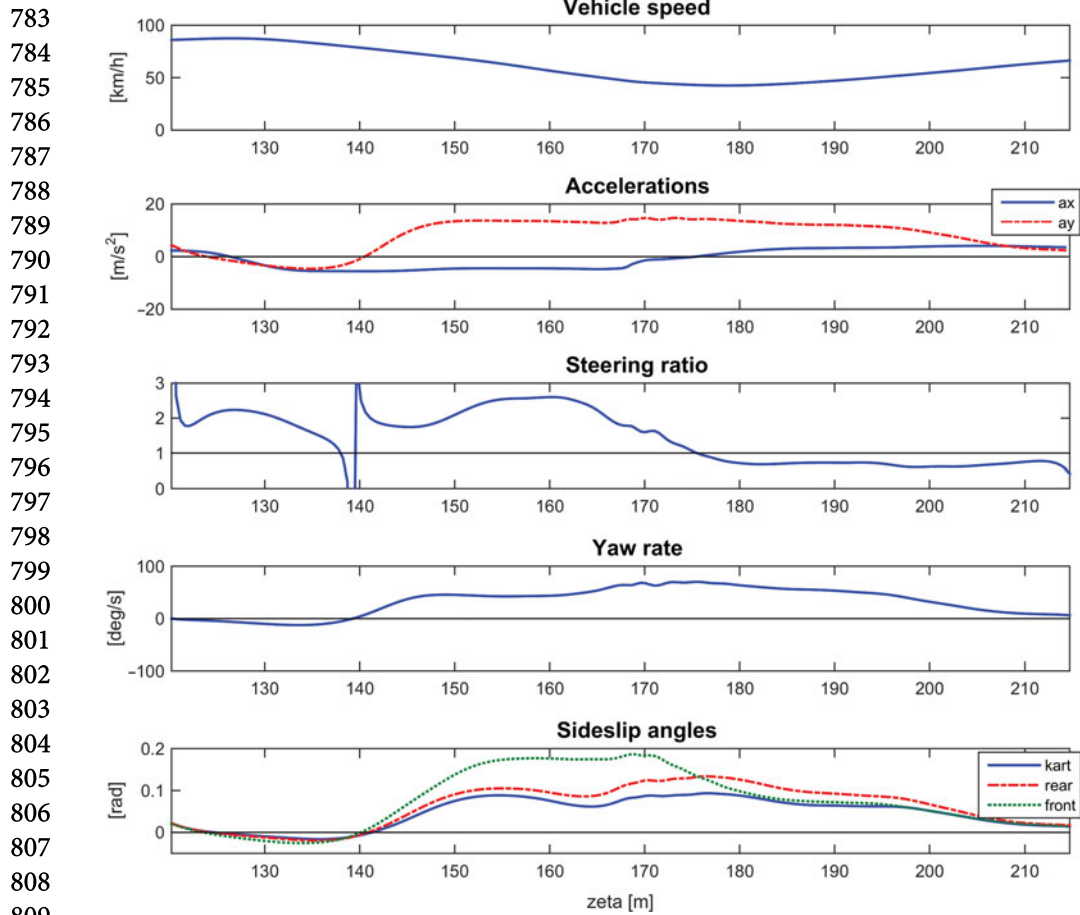
Figure 9. Turn analysis: gross-motion. Steering ratio shown in the chart *d* is the ratio between the real curvature radius and the kinematic one (that is the radius of curvature at zero slip). Values higher than 1 indicate that the vehicle is under-steering, lower than 1 over-steering. Rear (front) sideslip angle in figure (e) is the average of the rear (front) left and right tyres.

roughly associated with braking ($125 < s < 165$), cornering ($165 < s < 185$) and accelerating ($185 < s < 210$). The ratio between the real curvature radius and the kinematic one (steering ratio) is lower than one after the second half of the manoeuvre, when the vehicle is accelerating, and it is greater than one during all the rest of the time except for a short transient at turn entrance in correspondence with the *pendulum* manoeuvre. When the yaw rate passes through zero the steering ratio diverges to infinity since the kinematic curvature radius is zero. The under-steering behaviour of the kart at the entrance of the turn is confirmed also by Figure 9(e), which shows that the front tyres sideslip angle is almost the double of that of rear ones. The tyre slip and forces that are generated in this manoeuvre are shown in Figure 10. In the braking phase, longitudinal slips are obviously negative for both tyres and they are near the value at which the maximum of the (uncoupled) longitudinal force is exerted. The reason they do not reach such a value is because the longitudinal force is coupled with the lateral one that is also exerted at the same time.
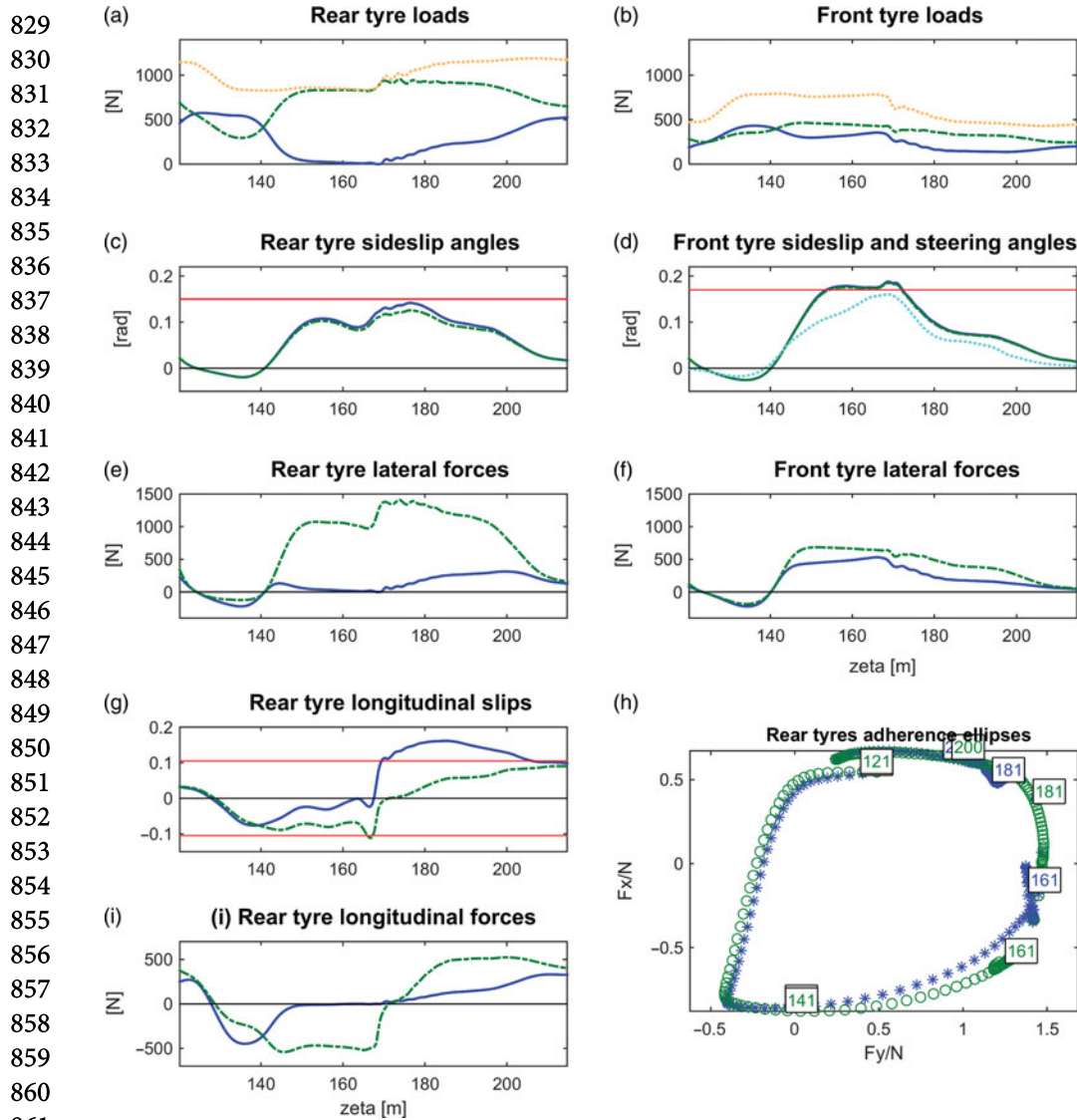
Figure 10. Turn analysis: tyres kinematic. Continuous blue lines refer to right tyres, dash-dot green ones to left tyres. Dotted orange lines, when present, show the sum of left and right tyres. Horizontal red lines in figure (c), (d) and (g) represent the value at which the maximum of tyre adherence is reached for a non-combined tyre force at nominal load. In plot (d), the dotted cyan line represents the steering angle. In figure (h), asterisks refer to right tyre, circles to left one; numbers within a rectangular box show the value of the curvilinear abscissa *s* of the point. Turn manoeuvre begins from the top of the picture and then continues counterclockwise. Tyre vertical loads in (a) and (b) clearly highlight how the right rear tyre (inner tyre) gets completely unload during the manoeuvre.

Then, while turning, the longitudinal slip of the two tyres shows significant differences due to the yaw motion (the absence of differential forces the wheels to have the same spin) and, since the yaw is positive, the right tyre has always a higher slip. When the kart has exited from the turn and the yaw rate is nearly zero, the longitudinal slip of the two tyres becomes equal again. Regarding the lateral slippage, the sideslip angles of rear tyres start increasing

875 from zero when the kart enters the curve, then they reach the maximum at the middle
876 of the turn and then decrease and become zero again when the kart has exited the turn.
877 The rear tyres never reach the maximum of pure lateral adherence. Concerning front tyres,
878 it can be noticed that the difference between right and left load is significant but as huge
879 as for rear tyres. This is a clear evidence that the steering effect transfers a considerable
880 load to the front inner wheel. The sideslip angles of front tyres have a trend that is almost
881 proportional to that of the steering angle (Figure 10(d), cyan line).

882 Adherence ellipses shown in the bottom-right corner of Figure 10 confirm what has
883 been said in the previous chapter: in every cornering only the outer tyre has the combina-
884 tion of longitudinal slip and sideslip angle engaging it to the limits of adherence ellipses.
885 Indeed, red points are arranged over a bigger ellipsoidal shape.

886 Finally, from the comparison of rear tyres longitudinal forces in Figure 10 with the steer-
887 ing ratio shown in Figure 9, it can be noticed that, at least as rough approximation, the
888 vehicle is under-steering when braking, and over-steering when accelerating. Keeping in
889 mind the longitudinal tyre force trend, this behaviour is reasonable: since most of the lon-
890 gitudinal force is exerted by the outer tyres (inner is less loaded), when braking such force
891 generates an aligning yaw torque, and a turning torque when accelerating.

6. Conclusions

In this work, we demonstrated the development of a multibody model for go-karts. First,
we presented the mathematical formulation of the multibody system together with optimal
control formulation. An indirect method was used to solve the optimal control problem
which allowed us to perform simulations. The model, fed with kart characteristics mea-
sured by lab tests, has been demonstrated to reproduce enough accurately the telemetry
recorded during the experimental track test with an expert driver. Speed and accelerations
measured resulted in very good agreement with simulated signals. Simulation results have
been exploited to study the dynamics of karts with particular attention to tyres dynamics.
We have been able to reproduce racing manoeuvres that bring to the lifting of the rear inner
wheel when turning. The importance of such manoeuvres due to the lack of differential has
been highlighted too.

With this work we developed a powerful tool that can be used to optimise kart charac-
teristic (such as frame and anti-roll bar stiffness) when designing such vehicles ; it allows
us to investigate how they affect vehicle manoeuvrability before to execute any track test.
Moreover, this model can be modified and used as a starting point for other four-wheeled
vehicles for optimal control problem. Even if in the literature other authors have presented
OCP simulations for cars [1] and Formula1 cars,[2] this work is among the first to calculate
the tyre loads from the vehicle dynamics and tyre deformations.

Further perspective can be the parametric analysis and optimisation of structural
characteristic.

Disclosure statement

No potential conflict of interest was reported by the authors.

References

[1] Tavernini D, Velenis E, Lot R, Massaro M. The optimality of the handbrake cornering technique. J Dyn Syst Meas Control. 2014;136:041019.
[2] Perantoni G, DJN Limebeer. Optimal control for a formula one car with variable parameters. Veh Syst Dyn. 2014;52:653–678.
[3] Sharp RS. A method for predicting minimum-time capability of a motorcycle on a racing circuit. J Dyn Syst Meas Control. 2014;136:041007.
[4] Simon B, Vittore C, Matteo M, Martino P. Application of the optimal maneuver method for enhancing racing motorcycle performance. SAE Technical Paper; 2008.
[5] Mirone G. Multi-body elastic simulation of a go-kart: correlation between frame stiffness and dynamic performance. Int J Automot Technol. 2010;11:461–469.
[6] Lot R, Da Lio M. A symbolic approach for automatic generation of the equations of motion of multibody systems. Multibody Syst Dyn. 2004;12:147–172.
[7] Bertolazzi E, Biral F, Da Lio M. Symbolic–numeric indirect method for solving optimal control problems for large multibody systems. Multibody Syst Dyn. 2005;13:233–252.
[8] Bertolazzi E, Biral F, Da Lio M. Symbolic–numeric efficient solution of optimal control problems for multibody systems. J Comput Applied Math. 2006;185:404–421.
[9] Pacejka H. Tire and vehicle dynamics . Oxford: Elsevier; 2006.
[10] Lot R, Biral F. A curvilinear abscissa approach for the lap time optimization of racing vehicles. In: World Congress, Vol. 19, 2014. p. 7559–7565.
[11] Viviani P, Flash T. Minimum-jerk, two-thirds power law, and isochrony: converging approaches to movement planning. J Exp Psychol: Human Percept Perform. 1995;21:32.
[12] Bryson A. Dynamic optimization. Reading, MA: Addison Wesley Longman; 1999.
[13] Pinch ER. Optimal control and the calculus of variations. Oxford: Oxford University Press; 1993.
[14] Cossalter V, Doria A, Lot R, Ruffo N, Salvador M. Dynamic properties of motorcycle and scooter tires: measurement and comparison. Veh Syst Dyn. 2003;39:329–352.
[15] Gillespie TD. *Fundamentals of vehicle dynamics*. SAE Technical Paper; 1992.

Q2

Q3

Appendix. Tyre parameters

Table A1. Pacejka's tyre magic formula coefficients.

Coefficient	Rear tyre	Front tyre
p_{Cx1}	2.3	
p_{Dx1}	0.9	
p_{Ex1}	0.95	
p_{Kx1}	20	
p_{Kx2}	1	
p_{Kx3}	−0.5	
p_{Cy1}	2.3	2.13
p_{Dy1}	1.5	1.5
p_{Ey1}	0.9	0.8
p_{Ky1}	−37.6	−34.1
p_{Ky2}	1.6	1.6
p_{rBx1}	14	
p_{rBy1}	12	
p_{rCy1}	0.6	
λ_{Fz0}	1.6	1.6

All Pacejka's coefficients ([9], chapter 4) that are not listed here have been set to their neutral value (either 0 or 1).